ACS OMEGA

Open Access

http://pubs.acs.org/journal/acsodf

Article

Bismuth, Nitrogen-Codoped Carbon Dots as a Dual-Read Optical Sensing Platform for Highly Sensitive, Ultrarapid, Ratiometric Detection of Doxorubicin

Fangfang Du,* Yuan Gao, Xibo Zhang, and Li-Li Wang*

Cite This: *ACS Omega* 2023, 8, 41383−41390

Read Online

ACCESS | Metrics & More | Article Recommendations | Supporting Information

ABSTRACT: Doxorubicin (DOX) is a potent anticancer drug, but it has side effects on normal tissues, particularly myocardial cells. Therefore, it is crucial to detect the DOX concentration in body fluids for effective clinical treatment. In this work, N,Bi-codoped CDs (Bi,N-CDs) were synthesized through a one-step hydrothermal method to carbonize the raw materials of 2,4-dinitroaniline and bismuth nitrate. The resulting Bi,N-CDs showed a reduced emission at 490 nm and an enhanced emission at 590 nm in the presence of DOX. The ratio of fluorescence (FL) intensity (F_{590}/F_{490}) was found to be a reliable indicator of DOX concentration, ranging from 0.05 to 30 μM and 40−200 μM, with detection limits (LOD) of 34 and 24 nM, respectively. A ratiometric fluorescence nanoprobe was established for highly selective and sensitive detection of DOX using a specific electrostatic interaction and inner filter effect between Bi,N-CDs and DOX. Meanwhile, Bi,N-CDs exhibited a distinct color change ranging from yellow to orange-red when exposed to DOX, allowing for a colorimetric method to measure DOX levels in the range of 0.05−30 μM, with a detection limit of 169 nM. The probe was triumphantly used to monitor DOX in actual samples via a dual-mode optical sensing strategy. This study contributes to the development of heteroatom-doped CDs and expands their potential applications for detecting biological samples.

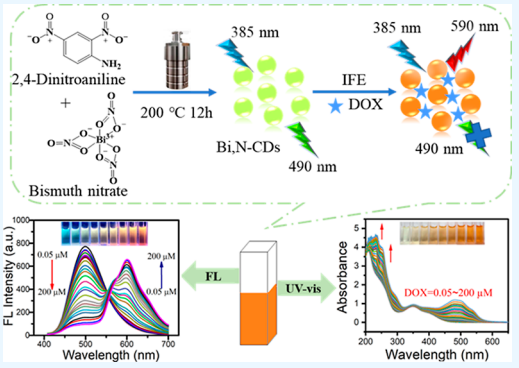

1. INTRODUCTION

Doxorubicin (DOX) is an effective chemotherapy drug among anthracycline antibiotics, which promotes cancer treatment through a variety of mechanisms, for example, by inserting DNA base pairs and interacting with Topoisomerase II to destroy DNA replication and repair.[1−3] However, Dox in cancer treatment is limited by two main factors: nonspecific toxicity and the emergence of tumor resistance. When cancer cells are inhibited, the function of normal cells is also affected, leading to irreversible toxic effects on organs, such as, heart, brain, and kidneys, and can be life-threatening in severe cases.[4] Among breast cancer patients treated with DOX, the maximum plasma concentration range is 3.6−11 μM; after 24 h, the concentration in plasma generally decreases to a low nanomolar range.[5] The concentration of DOX in the urine of patients taking DOX is mg L^{-1}. For example, Maliszewska et al. reported that the DOX concentration in urine collected from patients after 0−4 h of administration was 9.44−17.87 mg L^{-1}, and the concentration of DOX in urine was almost 95 times that in the patient's plasma.[6] Considering the toxicity of DOX and personalized treatment for patients, it is imperative to develop sensitive and reliable methods for detecting DOX concentration in human serum and urine to achieve the desired therapeutic effect.[7] So far, various technologies, including chromatography, mass spectrometry, electrochemistry, and spectroscopy, have been developed to measure DOX.[8] It is worth noting that, compared to other technologies, fluorescence and colorimetry methods have gained attention in detecting DOX due to their simplicity, high sensitivity, convenience, and visibility.[9−12]

Carbon dots (CDs) are a new type of "zero-dimensional" fluorescent carbon materials, which have received extensive attention since their accidental discovery in 2004.[13] CDs have broad applications in bioimaging, therapy, LED, catalysis, and sensing[14−18] because of their outstanding properties, including easy preparation, tunable FL emission, eminent photostability, and excellent biocompatibility.[19,20] The CDs-based sensors have been used for the detection of ions[21,22] and small moleculars;[23,24] however so far, most reported fluorescence sensors of CDs were based on signal variations to detect analytes through fluorescence quenching, resulting in poor reliability, low sensitivity, and false positives. Thus, the development of a ratiometric fluorescence sensor is extremely

Received: July 15, 2023
Accepted: September 22, 2023
Published: October 23, 2023

https://doi.org/10.1021/acsomega.3c05093
ACS Omega 2023, 8, 41383−41390

desirable. Dai et al.[25] designed a novel sensing platform composed of blue and yellow emissive carbon dots that displayed a ratiometric fluorescence response toward CS_2. Li et al.[26] developed iron, cobalt, and nitrogen-codoped CDs as a dual-signal biosensor to detect uric acid by a fluorescence and colorimetry method. The ratiometric fluorescence probe has emerged as a powerful tool for the precise and quantitative detection of various targets owing to its unique self-calibration function, which allows it to compensate for environmental and instrumental factors that could potentially interfere with the accuracy of the measurements.[27−30] In addition, the ratiometric fluorescence detection system has the advantage of multiple fluorescence color changes, making it easy to visualize. However, there are few reports on ratiometric and colorimetric dual-mode sensing DOX based on CDs. Zhu et al.[31] used plums as precursors to prepare PCQDs through a one-step hydrothermal method as a ratio fluorescence nanoprobe for the determination of DOX. Zhang et al.[32] utilized 11-mercaptoundecanoic acid-functionalized CDs as a fluorescence and colorimetric dual-mode sensor for detecting DOX. However, due to the multistep synthesis, low fluorescence quantum yield, and low sensitivity of these optical nanoprobes, it require urgent development of a simple and efficient ratiometric optical probe for highly sensitive and selective quantitation of DOX.

The incorporation of metallic elements into CDs offers a more powerful approach to modify their electronic structures, thereby enhancing photocatalytic activity and sensing specificity, which makes metallic heteroatoms-doped-CDs promising materials for various applications, including photocatalysis and sensing.[33,34] Herein, Bi,N-CDs were prepared by one-step hydrothermal treatment using 2,4-dinitroaniline and bismuth(III) nitrate as raw materials, which were used as reversible ratio fluorescent nanoprobes for the determination of DOX. The as-prepared Bi,N-CDs exhibit bright green fluorescence at 490 nm. Intriguingly, a unique dual-emission response displays a ratiometric FL variation (F_{590}/F_{490}) upon the introduction of DOX, which is ascribed to the electrostatic interaction of Bi^{3+} on the surface of Bi,N-CDs with DOX. In addition, a colorimetric probe was also used to detect DOX. Finally, the dual-read optical nanoprobe was resoundingly applied to the detection of DOX in artificial urine and human serum, indicating that the constructed probe has potential application prospects in bioanalysis. In contrast to the previously reported FL probes, this work has the following innovative points: (1) a dual-mode sensor based on Bi,N-CDs was ingeniously developed by hydrothermal treatment. (2) Bi,N-CDs achieved visual quantification of DOX with high sensitivity.

2. EXPERIMENTAL SECTION

2.1. Materials and Reagents. 2,4-dinitroaniline, bismuth(III) nitrate, some amino acids (L-cysteine/L-Cys, L-arginine/L-Arg, DL-homocysteine/DL-Hcy, D-cysteine/D-Cys, DL-cysteine/DL-Cys), and antibiotics (tetracycline/TC, oxytetracycline/OTC, chlortetracycline/CTC, ciprofloxacin/CIP, streptomycin/SM, erythromycin/ERY, chloramphenicol/CAP), and ammonium citrate (AC) were purchased from Energy Chemical Co., Ltd. (China).

2.2. Fabrication of Bi,N-CDs. In a Teflon-lined stainless autoclave, 0.2 g of 2,4-dinitroaniline and 0.1 g of bismuth(III) nitrate in 15 mL of ultrapure water were treated with ultrasonic waves for 10 min to ensure complete dissolution. Then, the resulting solution was heated to 200 °C for 10 h. After cooling to room temperature, the yellow-green solution was purified by centrifugation (8000 rpm, 10 min) and filtering (0.22 μm filter membrane). Then the powder of Bi,N-CDs was obtained by freeze-drying the aqueous solution.

2.3. Assay Procedure of DOX. A certain concentration of DOX solution (50 μL, in PBS buffer, pH 6) was added into Bi,N-CDs solution (2.0 mL). Then, the mixture solution was measured by UV−vis absorption and a fluorescence spectrofluorometer. The fluorescence intensities of Bi,N-CDs (F_{490}) and (F_{590}) and absorbance values (A_{235}) and (A_{255}) were recorded, and their ratios (F_{490}/F_{590}) and (A_{235}/A_{255}) were employed to quantify DOX. The selectivity of Bi,N-CDs toward DOX was investigated in the same way via the addition of potential interfering substances (amino acids, antibiotics, or metal salts).

2.4. Analysis of DOX in Real Samples. To explore the feasibility of nanoprobes for detecting DOX in real samples, artificial urine was purchased from Phygene Co., Ltd. (China), and human serum was collected from healthy adult volunteers. Artificial urine was filtered through a 0.22 μm filter membrane and diluted 100 times for later use. 7.5 mL of acetonitrile was mixed with 5 mL of human blood sample and centrifuged at 8000 rpm for 10 min. The mixture solution was evaporated to remove the solvent, dissolved in ultrapure water, and diluted 50 times. Sample analysis was conducted according to the above assay procedure.

3. RESULTS AND DISCUSSION

3.1. Characterization of Bi,N-CDs. Transmission electron microscopy (TEM) scanning image showed that Bi,N-CDs were spherical and uniform with average sizes of 6.22 ± 0.5 nm (Figure 1A,B). X-ray photoelectron spectroscopy (XPS) and

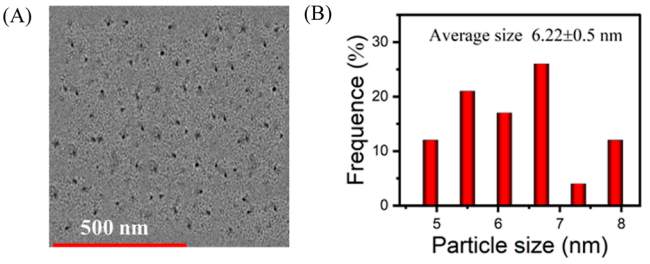

Figure 1. (A) TEM of Bi,N-CDs and (B) size distribution of Bi,N-CDs.

FTIR spectra were utilized to verify the compositions and surface functional groups of Bi,N-CDs. The full spectrum of XPS clearly shows four peaks at 168.5, 284.8, 400.5, and 532.2 eV, corresponding to Bi 4f, C 1s, N 1s, and O 1s, respectively (Figure 2A). The atomic ratios of these elements were calculated to be 0.04% Bi, 59.74% C, 12.88% N, and 27.34% O. The presence of Bi doping in Bi,N-CDs was verified by the observation of Bi $4f_{7/2}$ and Bi $4f_{5/2}$ peaks at 153.2 and 168.6 eV, respectively (Figure 2B).[35] The high-resolution spectrum of C 1s revealed three distinct binding energies at 284.5, 285.9, and 288.4 eV, which were assigned to C−C/C═C, C−O/C−N, and C═O bonds, respectively (Figure 2C).[36] The N 1s spectra of Bi,N-CDs could be decomposed into three peaks at 399.6, 401.2, and 406.1 eV (Figure 2D), corresponding to pyrrolic-N, N−H, and $-NO_3^-$ bonds, respectively.[37] The O 1s spectrum indicated the presence of C−O and N−O bonds at 531.7 and 533.0 eV, respectively (Figure S1).[38] These findings

https://doi.org/10.1021/acsomega.3c05093
ACS Omega 2023, 8, 41383−41390

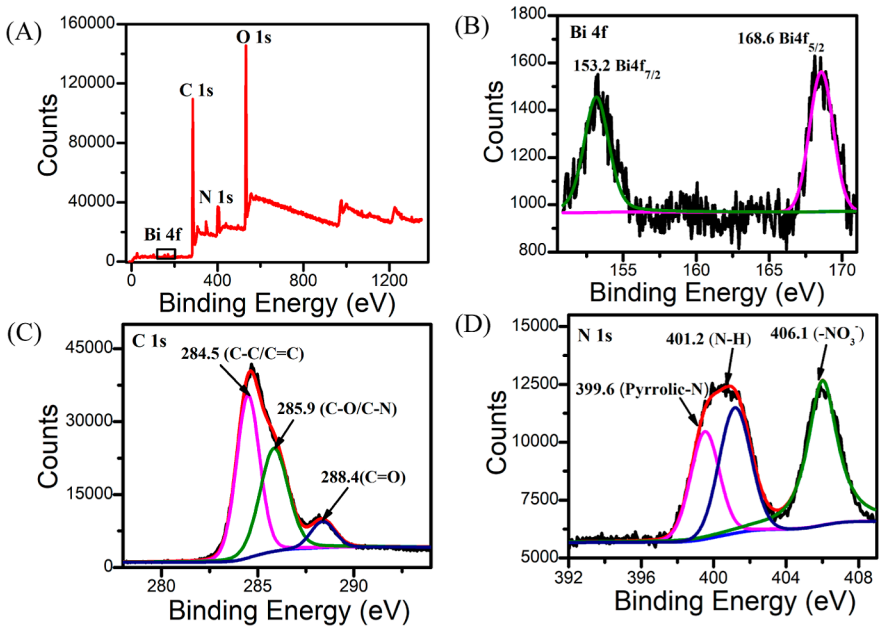

Figure 2. (A) Full-scan XPS images of Bi,N-CDs, (B) Bi 4f, (C) C 1s, and (D) N 1s.

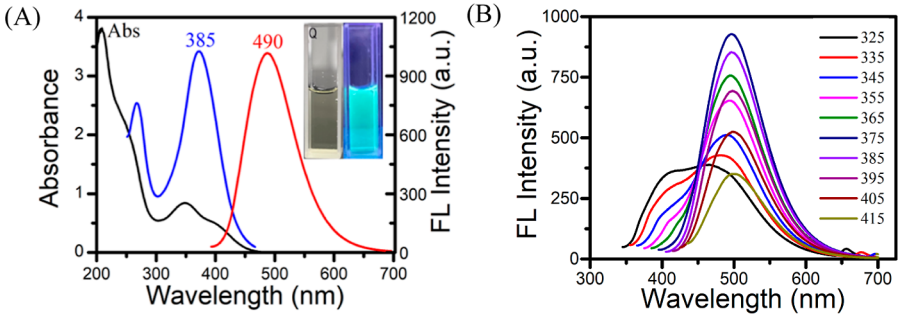

Figure 3. (A) UV−vis absorption spectra, optimal excitation, and FL emission spectra of Bi,N-CDs (inset: photographs under 365 nm UV light). (B) FL spectra of Bi,N-CDs with different λ_{ex} values from 325 to 415 nm.

were further supported by FTIR analysis, which showed characteristic stretching vibrations of O−H or N−H at 3451 cm^{-1}, $-NO_3^-$ at 1335 and 834 cm^{-1}, and C−N at 1335 and 834 cm^{-1} (Figure S2).[39] XPS and FTIR results provided a comprehensive understanding of the surface composition and functional groups on Bi,N-CDs (Figure 3).

3.2. Optical Properties of Bi,N-CDs. Figure 2A exhibits UV−vis absorption spectrum of Bi,N-CDs with two apparent absorption peaks at around 209 and 349 nm, corresponding to the $\pi-\pi^*$ transition of the aromatic C═C and the $n-\pi^*$ transition of functional groups, respectively.[40,41] The emission peak of Bi,N-CDs at 490 nm appears under an excitation wavelength of 385 nm with a Stokes shift of 105 nm. The Bi,N-CDs aqueous solution exhibits a strong green emission with FL quantum yields of 11.2%, which may be ascribed to the formation of aromatic π-conjugated structures (carbon core) or Bi^{3+} doping.[42,43] Bi,N-CDs display excitation-dependent FL characteristics (Figure 2B). As the excitation wavelength increased from 325 to 415 nm, the emission peak gradually shifted from 450 to 510 nm, accompanied by an intensity that increased first and then decreased, which is attributable to different sizes and surface state distributions of Bi, N-CDs.[44] In addition, the FL intensity of Bi,N-CDs gradually increases with the increase of Bi,N-CDs concentration from 0 to 0.037 mg/mL, indicating that Bi,N-CDs have a concentration-dependent fluorescence performance, and 0.033 mg/mL was chosen as the optimal detection concentration (Figure S3).

Photostability plays a crucial role in the sensitivity of fluorescence detection. Hence, the effects of pH, ionic strength, xenon lamp irradiation, storage time, and temperature on the FL intensity were investigated in detail. FL intensity of Bi,N-CDs remains steady over a wide pH range from 5 to 10 (Figure S4A) or under NaCl concentrations up to 2 M (Figure S4B), suggesting that Bi,N-CDs have pH stability and ionic strength resistance. Furthermore, Figure S4C shows that Bi,N-CDs exhibit minimal attenuation in FL intensity when exposed to xenon lamp irradiation for 15 min, demonstrating the strong photobleaching resistance of Bi,N-CDs. After 5 months of storage at 4 °C, the FL intensity of Bi,N-CDs remains 81.4%, indicating the excellent photostability of Bi,N-CDs (Figure S4D). These results collectively demonstrate the excellent stability of Bi,N-CDs, which lays a solid foundation for their potential applications in various fields. Figure S5A shows that the FL intensity gradually decreases as the temperature increases from 30 to 80 °C. 30 °C is the optimal temperature in common application environments. Figure S5B reveals that FL intensity has a good linear relationship with the temperatures. The corresponding regression equation is $y = -7.23x + 1377$ ($R^2 = 0.991$). The variations in FL were observed during successive heating and cooling cycles between

https://doi.org/10.1021/acsomega.3c05093
ACS Omega 2023, 8, 41383−41390

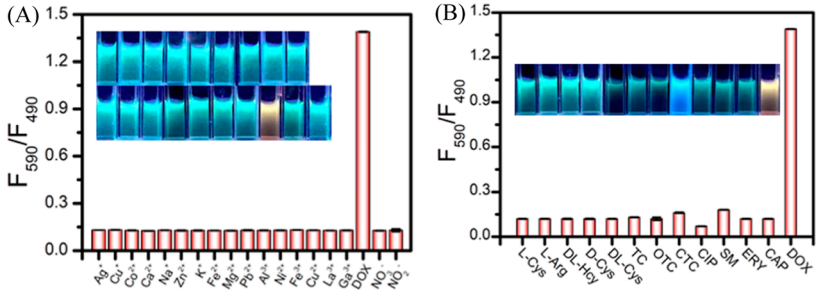

Figure 4. (A) Response of fluorescence intensity of Bi,N-CDs after the addition of DOX (0.5 mM), other different metal ions (0.5 mM), anions (0.5 mM), and (B) small-molecule substances (0.05 mM). Inset: photographs of the Bi,N-CDs after mixing with analytes under UV light.

30 and 80 °C (Figure S5C). The reversible process can be readily repeated for up to 5 cycles, and the FL intensity remains unchanged. The result suggests that Bi,N-CDs have excellent reversibility and restorability.

3.3. Dual-Read Assay for DOX Quantitation. To estimate the selectivity of DOX, several common metal cations (Ag^+, Ca^{2+}, Na^+, Zn^{2+}, K^+, Fe^{2+}, Mg^{2+}, Cu^{2+}, Fe^{3+}, etc.) (Figure 4A) and different amino acids (L-Cys, L-Arg, DL-Hcy, D-Cys, DL-Cys) and antibiotics (TC, OTC, CTC, CIP, SM, ERY, CAP) were investigated (Figure 4B). The inset of Figure 4 suggests that DOX and CIP can induce a significant fluorescence color change from green to orange and blue. The ratio of the FL intensity (F_{590}/F_{490}) at 590 nm (noted as F_{590}) and 490 nm (noted as F_{490}) exhibited a pronounced increase by the addition of DOX, but the influence of other analytes was negligible, suggesting that Bi,N-CDs have good selectivity for DOX.

Aiming at the optimal sensing performance of the fabricated Bi,N-CDs sensor for DOX, some vital parameters such as different pH values and reaction times of Bi,N-CDs with DOX were comprehensibly optimized. The effect of pH (3.0−9.0) on the FL intensity of Bi,N-CDs-DOX systems was investigated (Figure S6A). The FL intensity ratio (F_{590}/F_{490}) reached a maximum at pH 6, so this was selected as the optimum value for DOX detection. In addition, the effect of the reaction time during the determination of DOX was also investigated. Figure S6D displays that upon introduction of DOX into the Bi,N-CDs solution, the F_{590}/F_{490} value increases rapidly to reach a plateau within 5 s and remains stable for 1 min. Overall, Bi,N-CDs is an ultrarapid nanoprobe for monitoring the fluctuation of DOX.

The above optimal conditions were set for the ratiometric detection of DOX. As shown in Figure 5A, the emission intensity declined gradually at 490 nm and enhanced progressively at 590 nm with increasing DOX concentration. A linear relationship was observed between FL intensity ratios (F_{590}/F_{490}) and DOX concentrations in the range of 0−200 μM. The linear equations fitted in the range of 0.05−30 and 40−200 μM were $F_{590}/F_{490} = 0.0239C_{DOX} + 0.201$ (R^2 = 0.996) (Figure 5B) and $F_{590}/F_{490} = 0.0343C_{DOX} - 0.402$ (R^2 = 0.998) (Figure 5C), respectively. The detection limits were found to be 34 and 24 nM, respectively. The FL of Bi,N-CDs under a 365 nm UV lamp altered from green to orange-red upon introducing DOX, which is compatible with the CIE titration curve (Figure 5D). Additionally, the colorimetric signal response to DOX was observed. As depicted in Figure 5E, absorption peaks at 235, 255, and 290 nm and a wide peak in the range of 350−600 nm appeared with the addition of DOX and their absorbances increased with increasing DOX

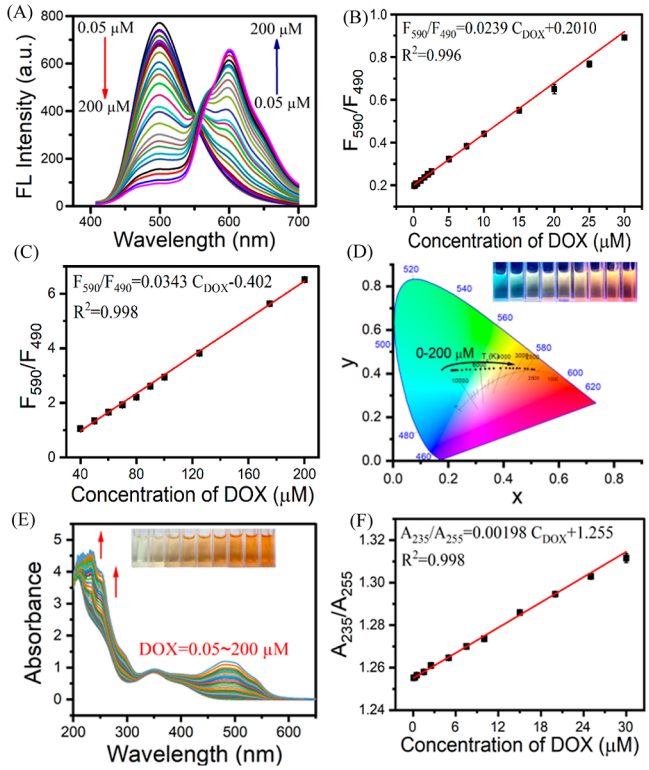

Figure 5. (A) Fluorescence spectra of the Bi,N-CDs with different DOX concentrations from 0.05 to 200 μM under λ_{ex} of 385 nm. Linear relationships of F_{590}/F_{490} versus different concentrations of DOX are in the ranges of (B) 0.05−30 and (C) 40−200 μM. (D) CIE chromaticity diagram of the Bi,N-CDs with different concentrations of DOX (0−200 μM). Inset: photographs of the Bi,N-CDs after mixing with different concentrations of DOX (5, 10, 20, 30, 40, 50, 75, 100, and 125 μM) under UV light. (E) UV−vis absorption spectra of the Bi,N-CDs with different concentrations of DOX (0.05−200 μM). Inset: photographs of Bi,N-CDs after mixing with different concentrations of DOX under visible light. (F) Linear relationship between the absorbance (A_{235}/A_{255}) of the Bi,N-CDs and the concentration of DOX is in the range of 0.05−30 μM.

concentration. The color of Bi,N-CDs under daylight changed from buff to orange. A ratiometric colorimetric probe was constructed by selecting the main peaks at 235 and 255 nm. A good linear relation between A_{235}/A_{255} and DOX concentration was observed (Figure 5F). The linear regression equation was $A_{235}/A_{255} = 0.00198C_{DOX} + 1.255$ (R^2 = 0.998) in the concentration range of 0.05−30 μM with a LOD of 169 nM. Compared to the previously reported CDs-based DOX sensors, the proposed nanosensor provides faster response times, wider linear ranges, and much lower LODs (Table

https://doi.org/10.1021/acsomega.3c05093
ACS Omega 2023, 8, 41383−41390

1).[31,32,45−47] The distinct color change of Bi,N-CDs with the gradual addition of DOX can be easily distinguished with the naked eye under UV light or sunlight. Therefore, N-CDs are capable of being considered as a highly sensitive nanoprobe for monitoring DOX using both fluorescence and colorimetry.

Table 1. Comparison of Proposed Material with Other Materials for DOX Detection

material	method	linear range (μM)	LOD (μM)	response time (s)	ref
PCQDs	fluorescence	1−30	0.12		27
		30−70			
MUA-CDs	fluorescence	0.25−19.96	0.66		28
	colorimetry	50.33−80.88	0.23		
		2.5−29.8	0.75		
PEI-CDs	fluorescence	0.1−150	0.075		38
NPCDs	fluorescence	0.5−6.5	0.012	600	39
R-CQDs	fluorescence	0.8−42.8	0.531	300	40
Bi,N-CDs	fluorescence	0.05−30	0.36	5	this work
	colorimetry	40−200	0.23		
		0.05−30	0.58		

3.4. Possible Sensing Mechanism. Subsequently, the sensing mechanism of DOX is discussed. Figure 6A exhibits that the absorption curve of the Bi,N-CDs and DOX mixture completely overlaps with the sum absorption curve (Bi,N-CDs + DOX), indicating a weak interaction between N-CDs and DOX without the formation of new functional groups. Furthermore, the excitation and emission spectra of Bi,N-CDs overlap with broad absorption spectra of DOX (Figure 6B), suggesting that Förster resonance energy transfer (FRET) or inner filter effect (IFE) may occur between Bi,N-CDs and DOX. To further confirm the quenching mechanism, the average FL lifetimes of Bi,N-CDs in the presence of DOX were investigated. As shown in Figure 6C, the FL lifetimes of Bi,N-CDs remained relatively constant with 4.89, 5.01, 4.88, and 4.89 ns with various concentrations of DOX (0, 50, 100, and 150 μM), indicating the presence of IFE. The zeta potential of Bi,N-CDs and the mixture of Bi,N-CDs-DOX were −1.05 and +11.01 mV (Figure S7), respectively, which may be attributed to the chelation between Bi^{3+} and hydroxyls or amino of DOX,[48] confirming the successful combination of Bi-CDs and DOX.

3.5. Reversibility of Bi,N-CDs. Some masking agents, including S^{2-}, $S_2O_3^{2-}$, SCN^-, GSH, EDTA, ammonium citrate (AC) and I^-, were added to the Bi,N-CDs to evaluate the reversibility of the interaction of DOX with Bi,N-CDs (Figure 7A). The system of Bi,N-CDs/DOX exhibits only a specific response to Na_2S. The FL intensity of Bi,N-CDs/DOX gradually strengthens at 490 nm and decreases at 590 nm with increasing concentrations of Na_2S (Figure 7B). Moreover, after the reversible cycle had been repeated four times, the FL intensity of the assay still measured 90.8% of the initial (F_{590}/F_{490}) value in the Bi,N-CDs/DOX system (Figure 7C). These results provide convincing evidence that the binding between DOX and Bi,N-CDs is a reversible process.

3.6. Application in Serum and Urine. The practical feasibility of Bi,N-CDs was verified by detecting the DOX content in human serum and urine using an optical dual-mode method (Tables 2 and S1). However, the values of DOX could not be detected in these real samples. The recoveries using the ratiometric fluorescent method were 92.8−99.1% with relative standard deviations (RSD) of 0.11−0.78%. Similarly, the recoveries using the colorimetric method were 91.1−102.9% with the RSD less than 0.15%. The results suggested that the nanoprobe has great potential in practical applications.

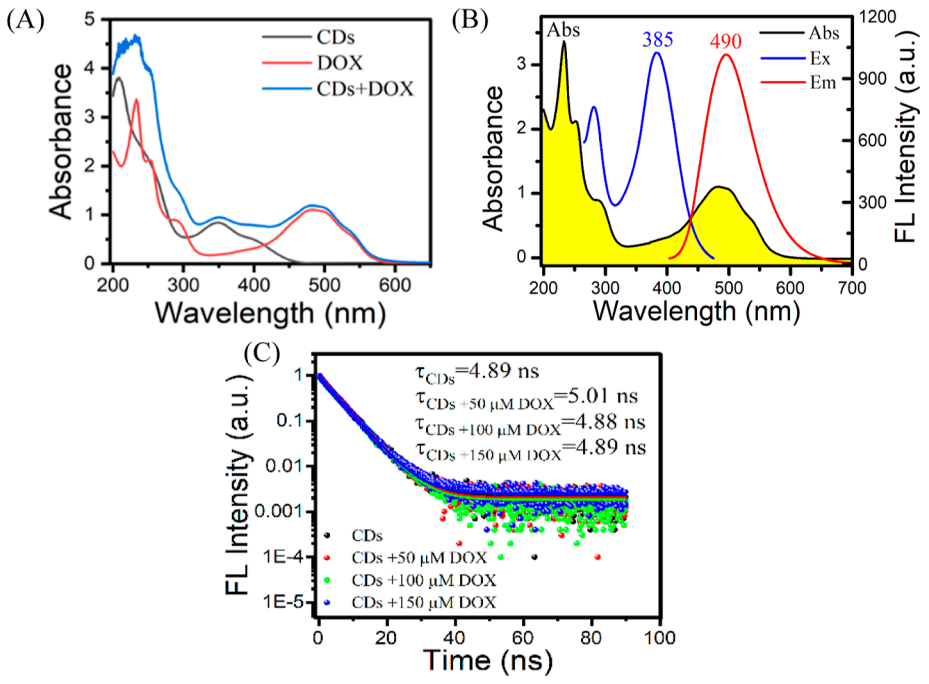

Figure 6. (A) UV−vis absorption spectrum of Bi,N-CDs, DOX, and Bi,N-CDs + DOX and (B) UV−vis absorption of DOX and fluorescence excitation and emission spectra of Bi,N-CDs. (C) PL decay profiles of Bi,N-CDs and Bi,N-CDs + DOX (50, 100, 150 μM).

https://doi.org/10.1021/acsomega.3c05093
ACS Omega 2023, 8, 41383−41390

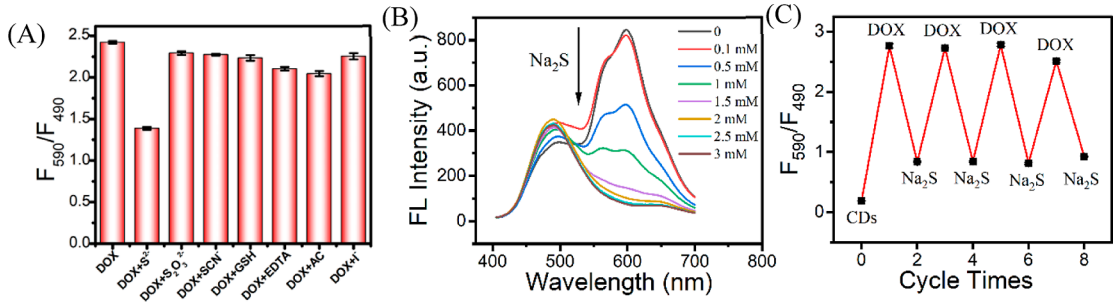

Figure 7. (A) Fluorescence intensity response of Bi,N-CDs/DOX (100 μM) mixture with 500 μM different masking agents [S^{2-}, $S_2O_3^{2-}$, SCN^-, GSH, EDTA, AC, and I^-]. (B) Fluorescence spectra of Bi,N-CDs/DOX with different concentrations of N_2S. (C) Reversible fluorescence response of Bi,N-CDs in cycles between Na_2S and DOX.

Table 2. Detection Results of DOX in Actual Samples by the Fluorescent Method

sample	spiked (μM)	found (μM)	recovery (%, n = 3)	RSD (%, n = 3)
artificial urine	10	9.33	93.3	0.45
	30	28.55	95.2	0.63
	50	49.54	99.1	0.11
human serum	75	72.74	97.0	0.73
	10	9.90	99.0	0.78
	30	28.48	94.9	0.24
	50	46.38	92.8	0.38
	75	70.24	93.7	0.75

4. CONCLUSIONS

In summary, A ratiometric fluorescence and colorimetry dual-read nano-sensor was established based on as-synthesized Bi,N-CDs for quantitative analysis of DOX according to specific electrostatic interaction and IFE. The sensor possesses some advantages of simple fabrication, high photostability, and ultrarapid quantitative ability. These characteristics endow them with a good prospect as nanosensors for the highly selective detection of DOX in real samples. Therefore, this study provides promising prospects for the development of multisignal sensing systems in future.

■ ASSOCIATED CONTENT

Supporting Information

The Supporting Information is available free of charge at https://pubs.acs.org/doi/10.1021/acsomega.3c05093.

Optimization of optical properties of fluorescence Bi,N-CDs and their performance as a sensor for detection of DOX, exhaustive structural characterization, change in zeta potential of Bi,N-CDs, and application of Bi,N-CDs in temperature sensing (PDF)

■ AUTHOR INFORMATION

Corresponding Authors

Fangfang Du − *School of Pharmaceutical Science, Postdoctoral Research Station of Basic Medicine, Hengyang Medical School, University of South China, Hengyang, Hunan 421001, China; Key Laboratory of Hainan Trauma and Disaster Rescue, The First Affiliated Hospital of Hainan Medical University and Engineering Research Center for Hainan Bio-Smart Materials and Bio-Medical Devices, Key Laboratory of Emergency and Trauma, Ministry of Education, Key Laboratory of Hainan Functional Materials and Molecular Imaging, College of Emergency and Trauma, Hainan Medical University, Haikou 571199, China;* orcid.org/0009-0000-9507-7171; Email: dfang@usc.edu.cn

Li-Li Wang − *School of Pharmaceutical Science, Postdoctoral Research Station of Basic Medicine, Hengyang Medical School, University of South China, Hengyang, Hunan 421001, China*; Email: wangll@usc.edu.cn

Authors

Yuan Gao − *School of Pharmaceutical Science, Postdoctoral Research Station of Basic Medicine, Hengyang Medical School, University of South China, Hengyang, Hunan 421001, China*

Xibo Zhang − *School of Pharmaceutical Science, Postdoctoral Research Station of Basic Medicine, Hengyang Medical School, University of South China, Hengyang, Hunan 421001, China*

Complete contact information is available at: https://pubs.acs.org/10.1021/acsomega.3c05093

Author Contributions

F.D. and Y.G. contributed equally to this work. F.D. was involved in the investigation, formal analysis, conceptualization, and writing of the original draft. Y.G. was involved in the investigation, validation, and data curation. X.Z. was involved in the investigation. L.-L.W. helped with funding acquisition, and writing−review and editing.

Notes

The authors declare no competing financial interest.

■ ACKNOWLEDGMENTS

This work was supported by the National Natural Science Foundation of China (no. 22174059), the Scientific Research Project of Hunan Provincial Health Commission (grant no. D202313027525), the Natural Science Foundation of Hunan Province (2022JJ40363), and the Excellent youth funding of Hunan Provincial Education Department (22B0460).

■ REFERENCES

(1) Lin, M.-Y.; Cheng, W.-T.; Cheng, H.-C.; Chou, W.-C.; Chen, H.-I.; Ou, H.-C.; Tsai, K.-L. Baicalin Enhances Chemosensitivity to Doxorubicin in Breast Cancer Cells via Upregulation of Oxidative Stress-Mediated Mitochondria-Dependent Apoptosis. *Antioxidants* **2021**, *10*, 1506.

(2) Lai, Y.-L.; Cheng, Y.-M.; Yen, S.-K. Doxorubicin-chitosan-hydroxyapatite composite coatings on titanium alloy for localized cancer therapy. *Mater. Sci. Eng., C* **2019**, *104*, 109953.

(3) Pan, H.; Yang, S.; Cheng, W.; Cai, Q.; Shubhra, Q. T. H. Alternate-day fasting exacerbates doxorubicin cardiotoxicity in cancer chemotherapy. *Trends Endocrinol. Metab.* **2023**, *34*, 392−394.
(4) Sritharan, S.; Sivalingam, N. A comprehensive review on time-tested anticancer drug doxorubicin. *Life Sci.* **2021**, *278*, 119527.
(5) Chekin, F.; Myshin, V.; Ye, R.; Melinte, S.; Singh, S. K.; Kurungot, S.; Boukherroub, R.; Szunerits, S. Graphene-modified electrodes for sensing doxorubicin hydrochloride in human plasma. *Anal. Bioanal. Chem.* **2019**, *411*, 1509−1516.
(6) Maliszewska, O.; Plenis, A.; Olędzka, I.; Kowalski, P.; Miękus, N.; Bień, E.; Krawczyk, M. A.; Adamkiewicz-Drożynska, E.; Bączek, T. Optimization of LC method for the quantification of doxorubicin in plasma and urine samples in view of pharmacokinetic, biomedical and drug monitoring therapy studies. *J. Pharm. Biomed. Anal.* **2018**, *158*, 376−385.
(7) Tacar, O.; Sriamornsak, P.; Dass, C. R. Doxorubicin: an update on anticancer molecular action, toxicity and novel drug delivery systems. *J. Pharm. Pharmacol.* **2012**, *65* (2), 157−170.
(8) Rong, S.; Zou, L.; Meng, L.; Yang, X.; Dai, J.; Wu, M.; Qiu, R.; Tian, Y.; Feng, X.; Ren, X.; Jia, L.; Jiang, L.; Hang, Y.; Ma, H.; Pan, H. Dual function metal-organic frameworks based ratiometric electrochemical sensor for detection of doxorubicin. *Anal. Chim. Acta* **2022**, *1196*, 339545.
(9) Zhang, R.; Liu, L.; Li, W.; Luo, X.; Wu, F. Luminescent carbon dots with excellent peroxidase mimicking property for fluorometric and colorimetric detection of glucose. *Colloids Surf., B* **2023**, *222*, 113125.
(10) Shen, Y.; Wei, Y.; Gao, X.; Nie, C.; Wang, J.; Wu, Y. Engineering an Enzymatic Cascade Catalytic Smartphone-Based Sensor for Onsite Visual Ratiometric Fluorescence-Colorimetric Dual-Mode Detection of Methyl Mercaptan. *Environ. Sci. Technol.* **2023**, *57*, 1680−1691.
(11) Wang, Q.; Tan, Q.; Zhao, S.; Zhang, K.; Chen, J.; Lan, M. Dual-responsive carbon dots-based luminophore for ratiometric fluorescence and room-temperature phosphorescence detection of oxytetracycline. *Chem. Eng. J.* **2023**, *470*, 144061.
(12) Guo, G.; Li, T.; Wang, Y.; Hu, H.; Xing, H.; Tang, S.; Gao, S.; Leng, X.; Chen, D. Aggregation-induced bimodal excitation of nitrogen-doped carbon dots for ratiometric sensing of new coccine and solid-state multicolor lighting. *J. Colloid Interface Sci.* **2023**, *645*, 96−106.
(13) Xu, X.; Ray, R.; Gu, Y.; Ploehn, H. J.; Gearheart, L.; Raker, K.; Scrivens, W. A. Electrophoretic Analysis and Purification of Fluorescent Single-Walled Carbon Nanotube Fragments. *J. Am. Chem. Soc.* **2004**, *126*, 12736−12737.
(14) Gao, F.; Liu, J.; Gong, P.; Yang, Y.; Jiang, Y. Carbon dots as potential antioxidants for the scavenging of multi-reactive oxygen and nitrogen species. *Chem. Eng. J.* **2023**, *462*, 142338.
(15) Jiang, L.; Cai, H.; Zhou, W.; Li, Z.; Zhang, L.; Bi, H. RNA-Targeting Carbon Dots for Live-Cell Imaging of Granule Dynamics. *Adv. Mater.* **2023**, *35*, 2210776.
(16) Zhao, W.-B.; Liu, K.-K.; Wang, Y.; Li, F.-K.; Guo, R.; Song, S.-Y.; Shan, C.-X. Antibacterial Carbon Dots: Mechanisms, Design, and Applications. *Adv. Healthcare Mater.* **2023**, *12*, 2300324.
(17) Wang, B.; Lu, S. The light of carbon dots: From mechanism to applications. *Matter* **2022**, *5*, 110−149.
(18) Zhang, C.; Chen, M.; Pan, Y.; Li, Y.; Wang, K.; Yuan, J.; Sun, Y.; Zhang, Q. Carbon Nanodots Memristor: An Emerging Candidate toward Artificial Biosynapse and Human Sensory Perception System. *Adv. Sci.* **2023**, *10*, 2207229.
(19) Yang, H.-L.; Bai, L.-F.; Geng, Z.-R.; Chen, H.; Xu, L.-T.; Xie, Y.-C.; Wang, D.-J.; Gu, H.-W.; Wang, X.-M. Carbon quantum dots: Preparation, optical properties, and biomedical applications. *Mater. Today Adv.* **2023**, *18*, 100376.
(20) Wang, Q.; Pang, E.; Tan, Q.; Zhao, S.; Yi, J.; Zeng, J.; Lan, M. Regulating photochemical properties of carbon dots for theranostic applications. *Wiley Interdiscip. Rev. Nanomed. Nanobiotechnol.* **2023**, *15*, No. e1862.
(21) Liu, Y.; Chen, J.; Xu, Z.; Liu, H.; Yuan, T.; Wang, X.; Wei, J.; Shi, Q. Detection of multiple metal ions in water with a fluorescence sensor based on carbon quantum dots assisted by stepwise prediction and machine learning. *Environ. Chem. Lett.* **2022**, *20*, 3415−3420.
(22) Jain, S.; Dilbaghi, N.; Kumar Singhal, N.; Kaushik, A.; Kim, K.-H.; Kumar, S. Carbon quantum dots@metal-organic framework based catalytic nucleic acid fluorescent system for highly sensitive and selective detection of Pb2+ in aqueous solutions. *Chem. Eng. J.* **2023**, *457*, 141375.
(23) Rasheed, T. Carbon dots as robust class of sustainable and environment friendlier nano/optical sensors for pesticide recognition from wastewater. *TrAC, Trends Anal. Chem.* **2023**, *160*, 116957.
(24) Lu, W.; Guo, Y.; Yue, Y.; Zhang, J.; Fan, L.; Li, F.; Zhao, Y.; Dong, C.; Shuang, S. Smartphone-assisted colorimetric sensing platform based on molybdenum-doped carbon dots nanozyme for visual monitoring of ampicillin. *Chem. Eng. J.* **2023**, *468*, 143615.
(25) Dai, R.; Chen, X.; Hu, Y. Ratiometric fluorescence determination of carbon disulfide in water using surface functionalized carbon dots. *Sens. Actuators, B* **2023**, *382*, 133499.
(26) Li, F.; Chen, J.; Wen, J.; Peng, Y.; Tang, X.; Qiu, P. Ratiometric fluorescence and colorimetric detection for uric acid using bifunctional carbon dots. *Sens. Actuators, B* **2022**, *369*, 132381.
(27) Ma, R.; Fu, L.; Long, N.; Guo, H.; Hou, Y.; Li, Y.; Li, P.; Wang, J.; Zhou, L.; Kong, W. Gold Nanoclusters and Silica-Coated Carbon Dots-Assisted Ratiometric Fluorescent Nanosensors for Ultrasensitive Detection of Glyphosate. *ACS Sustainable Chem. Eng.* **2023**, *11*, 5093−5104.
(28) Yao, H.; Li, S.-Y.; Zhang, H.; Pang, X.-Y.; Lu, J. L.; Chen, C.; Jiang, W.; Yang, L. P.; Wang, L. L. Tetralactam macrocycle based indicator displacement assay for colorimetric and fluorometric dual-mode detection of urinary uric acid. *Chem. Commun.* **2023**, *59*, 5411−5414.
(29) Deng, J.; Xu, J.; Ouyang, M.; Zou, Z.; Lei, Y.; Li, J.; Qing, Z.; Yang, R. Target-triggered hairpin-free chain-branching growth of DNA dendrimers for contrast-enhanced imaging in living cells by avoiding signal dispersion. *Chin. Chem. Lett.* **2022**, *33*, 773−777.
(30) Tang, S.; Wang, Y.; Guo, G.; Li, T.; Xing, H.; Hu, H.; Leng, X.; Gu, C.; Chen, D. Activated cascade effect for dual-mode ratiometric and smartphone-assisted visual detection of curcumin and F- based on nitrogen-doped carbon dots. *Sci. Total Environ.* **2023**, *872*, 162277.
(31) Zhu, J.; Chu, H.; Shen, J.; Wang, C.; Wei, Y. Green preparation of carbon dots from plum as a ratiometric fluorescent probe for detection of doxorubicin. *Opt. Mater.* **2021**, *114*, 110941.
(32) Zhang, L.; Xing, H.; Liu, W.; Wang, Z.; Hao, Y.; Wang, H.; Dong, W.; Liu, Y.; Shuang, S.; Dong, C.; Gong, X. 11-Mercaptoundecanoic Acid-Functionalized Carbon Dots As a Ratiometric Optical Probe for Doxorubicin Detection. *ACS Appl. Nano Mater.* **2021**, *4*, 13734−13746.
(33) Ma, X.; Ou, Q.; Yuan, J.; Yang, J.; Xu, S.; Zhang, X. Multifunctional Fe-doped carbon dots and metal-organic frameworks nanoreactor for cascade degradation and detection of organophosphorus pesticides. *Chem. Eng. J.* **2023**, *464*, 142480.
(34) Zhu, P.; Liu, Y.; Tang, Y.; Zhu, S.; Liu, X.; Yin, L.; Liu, Q.; Yu, Z.; Xu, Q.; Luo, D.; et al. Bi-doped carbon quantum dots functionalized liposomes with fluorescence visualization imaging for tumor diagnosis and treatment. *Chin. Chem. Lett.* **2023**, *108689*, 108689.
(35) Tu, H.; Li, S.; Luo, Z.; Xu, L.; Zhang, H.; Xiang, Y.; Deng, W.; Zou, G.; Hou, H.; Ji, X. Bi-doped carbon dots for a stable lithium metal anode. *Chem. Commun.* **2022**, *58*, 6449−6452.
(36) Arkin, K.; Zheng, Y.; Bei, Y.; Ma, X.; Che, W.; Shang, Q. Construction of dual-channel ratio sensing platform and molecular logic gate for visual detection of oxytetracycline based on biomass carbon dots prepared from cherry tomatoes stalk. *Chem. Eng. J.* **2023**, *464*, 142552.
(37) Iqbal, P.; Critchley, K.; Attwood, D.; Tunnicliffe, D.; Evans, S. D.; Preece, J. A. Chemical Manipulation by X-rays of Functionalized Thiolate Self-Assembled Monolayers on Au. *Langmuir* **2008**, *24*, 13969−13976.

https://doi.org/10.1021/acsomega.3c05093
ACS Omega 2023, 8, 41383−41390

(38) Ren, Y.; Fan, Z. Synthesis of fluorescent probe based on molecularly imprinted polymers on nitrogen-doped carbon dots for determination of tobramycin in milk. *Food Chem.* **2023**, *416*, 135792.
(39) Prince, S.; Suthan, T.; Gnanasambandam, C. Growth and Characterization of Organic 2,4-Dinitroaniline Single Crystals for Optical Applications. *J. Electron. Mater.* **2022**, *51*, 1639−1652.
(40) Jia, Y.; Cheng, Z.; Wang, G.; Shuang, S.; Zhou, Y.; Dong, C.; Du, F. Nitrogen doped biomass derived carbon dots as a fluorescence dual-mode sensing platform for detection of tetracyclines in biological and food samples. *Food Chem.* **2023**, *402*, 134245.
(41) Wang, D.; Zhang, L.-J.; Liu, M.-H.; Du, F.-F.; Shen, Z.-Y.; He, L.; Wang, L.-L. Aggregation enhanced FRET: A simple but efficient strategy for the ratiometric detection of uranyl ion. *J. Hazard. Mater.* **2023**, *454*, 131497.
(42) Qi, B. P.; Hu, H. H.; Bao, L.; Zhang, Z. L.; Tang, B.; Peng, Y.; Wang, B. S.; Pang, D. W. an efficient edge-functionalization method to tune the photoluminescence of graphene quantum dots. *Nanoscale* **2015**, *7*, 5969−5973.
(43) Wei, J.; Gao, J.; Liu, Y.; Zheng, G.; Wang, R. Rapid preparation of homogeneous carbon dots with yellow fluorescence and formation mechanistic investigation. *J. Nanopart. Res.* **2019**, *21*, 74.
(44) Li, J.; Gong, X. The Emerging Development of Multicolor Carbon Dots. *Small* **2022**, *18*, 2205099.
(45) Yang, M.; Yan, Y.; Liu, E.; Hu, X.; Hao, H.; Fan, J. Polyethyleneimine-functionalized carbon dots as a fluorescent probe for doxorubicin hydrochloride by an inner filter effect. *Opt. Mater.* **2021**, *112*, 110743.
(46) Zhang, W.; Ma, R.; Gu, S.; Zhang, L.; Li, N.; Qiao, J. Nitrogen and phosphorus co-doped carbon dots as an effective fluorescence probe for the detection of doxorubicin and cell imaging. *Opt. Mater.* **2022**, *128*, 112323.
(47) Li, Z.; Zhou, Z.; Wang, J.; Sun, Q.; Zhang, J.; Tao, T.; Fu, Y. Ratiometric fluorescence detection of doxorubicin by R-CQDs based on the inner filter effect and fluorescence resonance energy transfer. *New J. Chem.* **2023**, *47*, 3541−3548.
(48) Guo, J.; Lu, W.; Zhang, H.; Meng, Y.; Du, F.; Shuang, S.; Dong, C. Copper doped carbon dots as the multi-functional fluorescent sensing platform for tetracyclines and pH. *Sens. Actuators, B* **2021**, *330*, 129360.

https://doi.org/10.1021/acsomega.3c05093
ACS Omega 2023, 8, 41383−41390